



Eidgenössische Technische Hochschule Zürich
Swiss Federal Institute of Technology Zurich

Detection of fluorescence from ablated ^9Be for future implementation in a Penning trap

by
Igor Zhuravlev

under supervision of
Tobias Sägesser, Shreyans Jain and Dr. Pavel Hrmó

Prof. Dr. Jonathan Home
Trapped Ion Quantum Information Group

ETH Zürich, Department of Physics
Institute for Quantum Electronics

September, 2021

Contents

Abstract	3
1 Introduction	3
2 Experimental setup	3
2.1 Ablation laser	3
2.2 Photo-ionization laser	4
2.3 Vacuum chamber	4
2.4 Setup scheme	6
3 System control	7
4 Measurements	7
4.1 Ablation beam parameters	7
4.2 Oven tests	8
4.3 Ablation without collimator	9
4.4 Ablation with collimator	11
5 Discussion	12
5.1 Speed distribution	12
5.2 Ablation threshold	13
6 Conclusion	14

Abstract

In this paper we present the producing of neutral ^9Be atoms using ablation. With the help of the written program code, the entire experiment is performed by remote control of the laser trigger. The fluorescence signal of neutral beryllium in a vacuum chamber was detected using PMT. The necessary minimum power of an atomic oven and the ablation laser were measured to produce neutral atoms with acceptable for trapping velocities. The parameters of the ablation laser beam are also provided.

1 Introduction

In the endeavor to build a quantum computer, several competing platforms have emerged that can implement certain quantum algorithms using a few qubits [1]. Trapped atomic ions are among the most successful platforms for these purposes. Primarily, radio-frequency traps have been used to control multiple trapped-ion qubits in which the dynamic electric field is used to trap charged particles. Penning traps have been used to perform quantum simulations with two-dimensional (2D) ion crystals [2]. At present, most ion traps are loaded by electron bombardment or photo-ionization of a neutral atomic beam. Atoms are typically emitted from a resistively heated oven. In this case the atomic beam is continuous and cannot be rapidly switched on since it takes a while to heat up the oven wire. After switching off, some part of the atoms can still pass through the trap. Over time this can lead to the build up of material on trap electrodes and nearby surfaces which can cause the generation of stray electric fields. Also the vacuum at the trap gets worse in this case. An atom source that can be more rapidly turned on and off to provide a better controlled atom flux than a traditional thermal source is therefore highly desirable. Here we present an alternative technique of producing neutral atoms that can be used for the future loading into Penning trap.

In our experiment a pulsed laser source is used to ablate material from a beryllium metal wire. The produced atoms are directed through the future trap area, where they are photo-ionized. Through rapid triggering of the ablation laser, atoms can be produced in brief pulses only when required. This reduces the overall amount of material passing through the real trap and so reduces electrode contamination.

2 Experimental setup

2.1 Ablation laser

The Q-switched Nd:YAG¹ laser at a wavelength of 532 nm will be used as an ablation laser. In external trigger mode, it is capable of producing pulses with repetition rate of 1 to 15 Hz and a pulsewidth of 3–5 ns. The laser has a variable attenuator that allows you to control the pulse power. There are also normal and low power modes of operation. We will mainly make all measurements in the normal power. For more accurate control, we will fix the position of variable attenuator at the middle of the power bar and change the power using a $\lambda/2$ wave plate and PBS. Thus we can change the average pulse energy in the range of 0.2–1.4 mJ.

For safety reasons and due to the rather rapid increase in power as you move along the power bar, the position of variable attenuator will not go further than the median position during the experiment.

¹Continuum Minilite II

2.2 Photo-ionization laser

Photo-ionization of neutral beryllium occurs on the $2s^2\ ^1S_0 \rightarrow 2s2p\ ^1P_1$ transition near the wavelength of 235 nm [3]. For this purpose we will use Toptica diode laser at 470 nm which is frequency doubled to 235 nm through a nonlinear crystal. The PI laser power varied from 1.5 to 2.5 mW. Throughout the experiment we kept the laser in single mode operation.

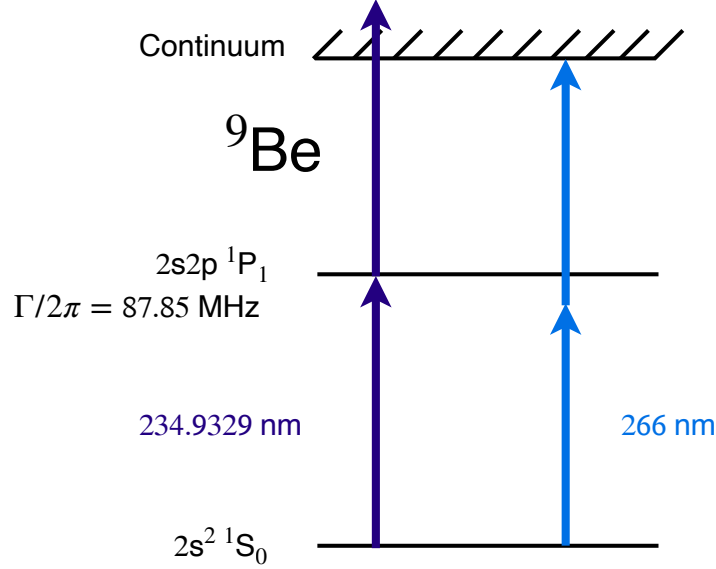


Figure 1: Levels and transitions used for a resonant excitation at 235 nm and subsequent non-resonant ionization in neutral beryllium, for non-resonant two-photon ionization at 266 nm, hyperfine and Zeeman sublevels not shown [4].

2.3 Vacuum chamber

A wire holder shown on the Fig. 2 is installed inside the vacuum chamber which is an aluminum chamber with three windows pumped out to a pressure $3\text{--}4 \times 10^{-6}$ mbar using a turbo-molecular pump.

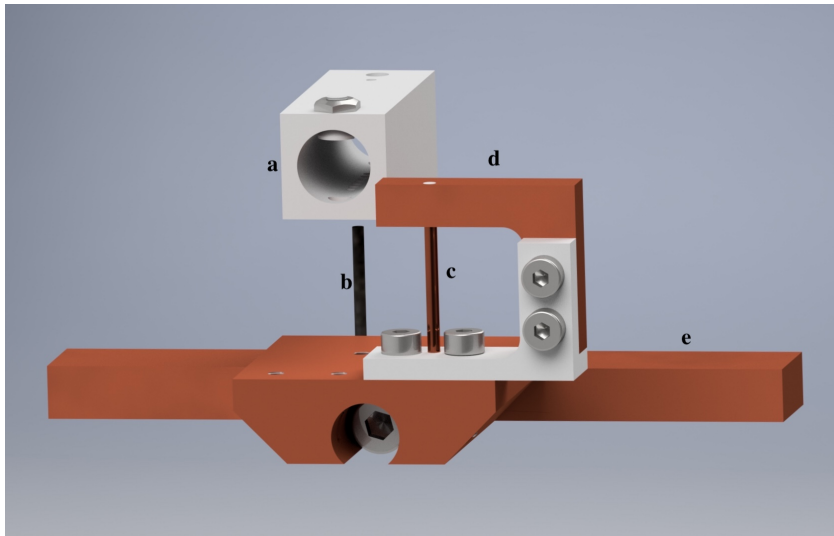


Figure 2: Ablation target mount: **a** – oven shield, **b** - needle, **c** – beryllium target, **d** – wire holder, **e** – guide bar

The guide bar is fixed in the middle of the chamber and has a metal needle in the center. There is also a lens inside the chamber on the right edge of the bar which collimates the output fluorescence light [5]. It is fixed on the bar and the center of the lens is aligned with the top of the needle. Hence it is a simple way to find out which point of the chamber we observe. Under the action of the ablation laser beryllium atoms propagate in distribution of directions around the target surface normal. Thus we just need to adjust the PI laser beam to point above the top of the needle. In addition to the ablation target the chamber also has a classic resistively heated oven which is surrounded by a shield with vertical holes and located exactly above the needle. This allows us to use evaporated atoms to check the proper operation of the detection system.

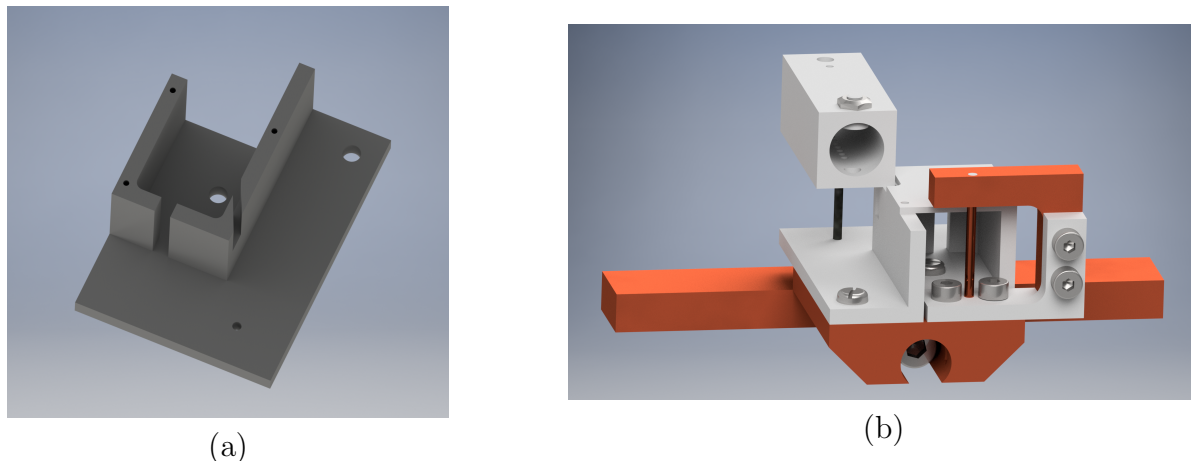


Figure 3: (a) – collimator, (b) – ablation target mount with collimator and cover

Due to not knowing the exact geometry of the atomic beam we can assume that the components of the velocity vector parallel to the PI laser k vector can be quite diverse. Since the Doppler shift depends on the direction of the velocity of the atoms relative to the direction of the PI laser beam we would like to select some specific direction of the atoms to observe a clear fluorescence signal. For this purpose we designed the collimator which is shown in Fig. 3. The selected direction for the needle is about 25° from the direction of PI laser which is close to the proposed value for the planned Penning trap experiment. The collimator also blocks all other directions of propagation of the atomic beam, so we will be able to observe the fluorescence of only those atoms that propagate at the fixed angle. This should help to restrict the range of frequency shifts and reduce unwanted signal. The images of the collimator and the ablation target mount are shown in Fig. 4.

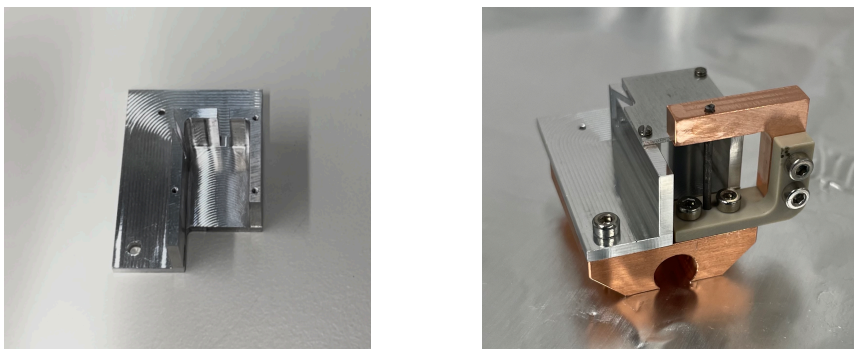


Figure 4: Collimator with the cover and the ablation target mount

2.4 Setup scheme

The laser beam geometry is shown in Fig. 5. The ablation laser beam passes through the $\lambda/2$ wave plate and then through the PBS in order to precisely adjust its power. It is then focused using a lens with $f = 200$ mm on the ablation target. A flip mirror is installed in front of the chamber to swap the beam from the power meter to the chamber. The PI laser goes straight into the chamber and is aligned with the top of the needle passing through the atomic beam and photo-ionizing it.

A lens with $f = 35$ mm is installed inside the chamber and collimates the fluorescence light passing through it. Then the light passes through a UV bandpass filter and focuses on a PMT with a lens with $f = 50$ mm.

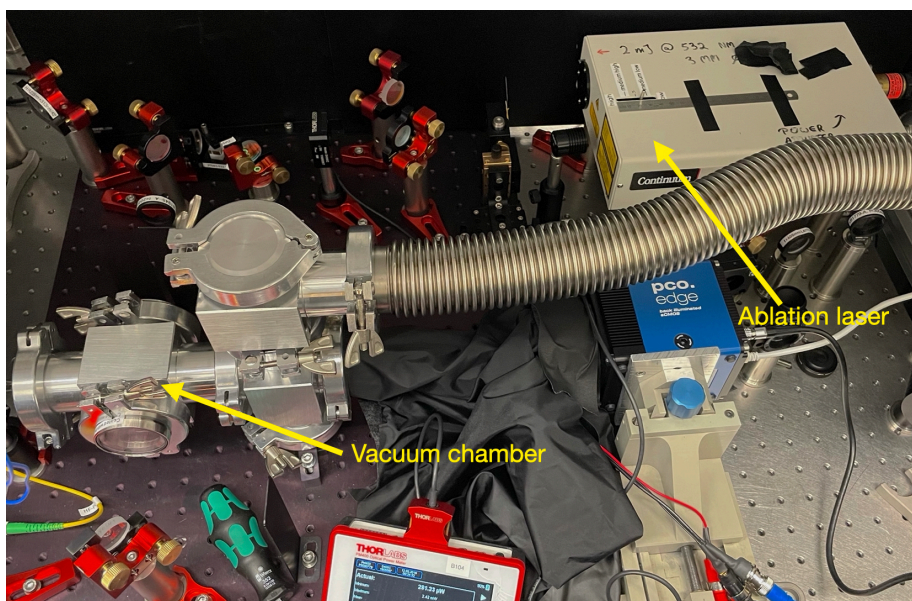
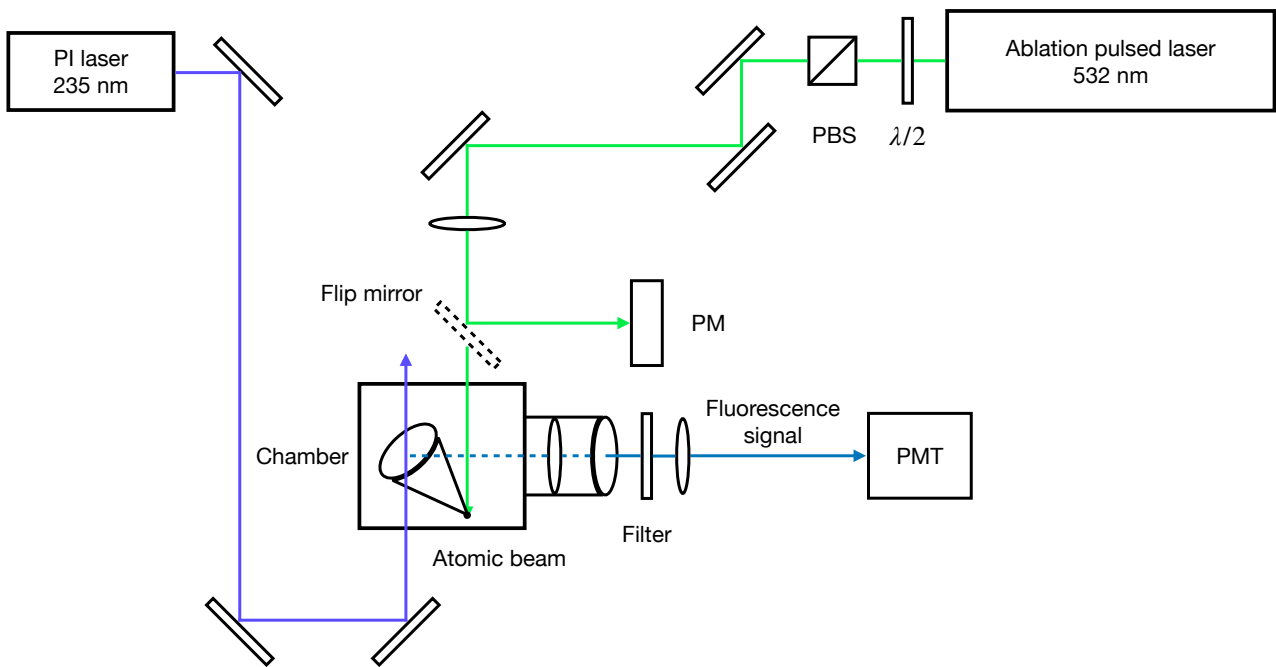


Figure 5: Experimental setup scheme (top) and installation image (bottom)

3 System control

The majority of the experiment with the exception of adjustment and manual parameter changes was carried out remotely. In order to control the pulsed laser and acquire data automatically, we wrote a Python script. It allows us to operate the laboratory equipment through a control software implemented in C++ (Ionizer). In the rear of the laser’s power supply, we set the flashlamp trigger to be external and the Q-switch source to be internal. The TRIG IN port of the flashlamp source is connected to a TTL channel through a BNC cable. With this setup, the pulsed laser could be externally triggered by a voltage pulse through the TTL interface. The scheme of the experimental processes is shown in Fig. 6.

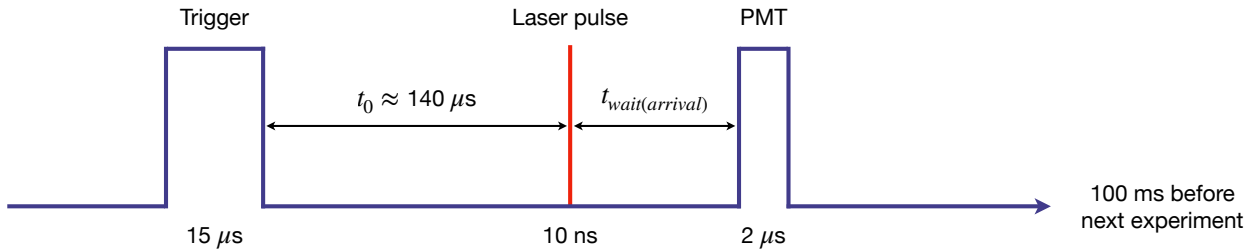


Figure 6: Sequence for analysing ablated neutral atom plume.

A trigger pulse is sent from the DDS board to the flashlamp in the laser head, through the TTL trigger pulse. After a latency of around 140 μs, the laser pulse will be emitted. Then we detect the fluorescence signal from the PMT within a detection window of 2 μs. After that we need to wait 100 ms before the next experiment due to the low limit of the laser’s repetition rate. Our Python script also allows us scan the frequency of the PI laser and the wait time t_{wait} after the TTL trigger.

4 Measurements

4.1 Ablation beam parameters

Since we want to ablate using the least amount of laser power, we need to focus the laser beam making the beam size commensurate with the size of the ablation target. For this purpose we use a lens with a focal length $f = 200 \text{ mm}$. Due to the lack of a beam profiler for the pulsed laser, we will use the knife-edge test for locating a focus and measuring the beam waist diameter. To do this, we will install the knife at various distances from the lens and gradually block the beam, while measuring the average laser power for each micro-step of the knife. Also, we used a thermal power sensor² instead of a photodiode and got the average value from the power meter within 20 seconds of measurements with an integration time of 10 ms and a pulse repetition rate of 10 Hz. The beam power $P(x, z)$ detected by the photodiode as a function of the knife-edge’s transverse position x and axial position z is obtained by integrating the Gaussian beam irradiance profile over all y and the unobstructed range of x . The result is

$$P(x, z) = p(z) \int_x^\infty \exp\left[-\frac{2(\xi - x_0)^2}{w^2(z)}\right] d\xi = \frac{P_0}{2} \operatorname{erfc}\left[\frac{\sqrt{2}(x - x_0)}{w(z)}\right], \quad (1)$$

²Thorlabs S470C

where

$$w(z) = w_0 \sqrt{1 + \left(\frac{M^2 \lambda (z - z_0)}{\pi w_0^2} \right)^2} = w_0 \sqrt{1 + \left(\theta \frac{(z - z_0)}{w_0^2} \right)^2}. \quad (2)$$

Thus approximating the experimental power data of the curve described by equation (1), we obtain a series of values of the beam radius at various points of the z axis. Using the obtained radius values and equation (2), we can determine the parameters z_0 , w_0 and M^2 . The pulsed laser has two power modes. Since the normal power mode has less power instability, we will make all measurements in this mode. The results of a least squares fit are shown in Fig. 7.

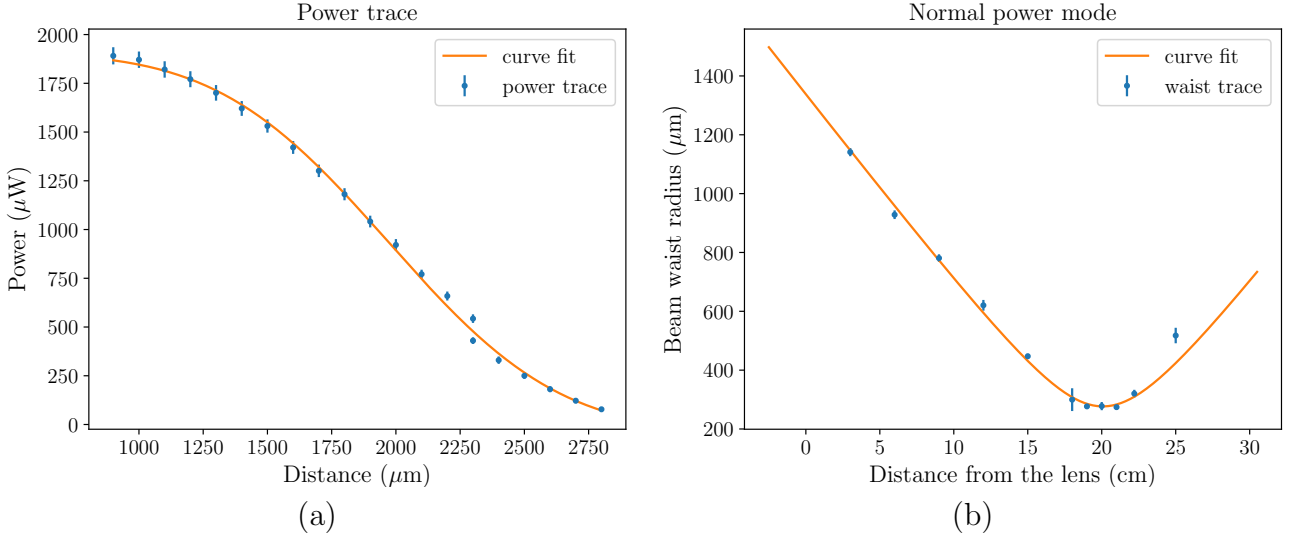


Figure 7: (a) – Fitting the power data with equation (1), (b) – approximation of waist radius values using equation (2).

The error bars on the plots are taken from the standard deviations of power obtained by the power meter. The `scipy.optimize.curve_fit` function of the Python - `scipy` standard library is used to obtain standard errors of the output parameters of the function. Thus, the following results were obtained

w_0 (μm)	z_0 (cm)	M^2
276 ± 8	20.1 ± 0.1	10.65 ± 0.06

where w_0 is a waist radius in the focus, z_0 is the focus distance of the lens and M^2 is a beam quality factor that represents the degree of variation of a beam from an ideal Gaussian beam.

4.2 Oven tests

To make sure that the detection system is working properly, we performed fluorescence measurements based on beryllium atoms evaporated from an effusive oven. Using the written Python script, we will scan the PI laser frequency near the resonant one ($f_0 = 638\,040\,044$ MHz). To do this, we will set laser frequency at the resonance and then scan the voltage on the piezoelectric element of the laser with an amplitude of 1.2 V. On every step we set the piezo voltage then wait for 0.5 s. After that we read the frequency from the wavelength meter³ and run an Ionizer experiment with a detection time of 200 μs . For every point in Fig. 8 we perform

³HighFinesse WS8-10, 10 MHz absolute accuracy, 400 kHz resolution

50 experiments. By varying the oven current, we found a suitable value for observing a clean fluorescence signal. We chose the current of 1.198 A while the minimum current for observing any signal was around 0.95 A for our oven wire. In Fig. 8(a) we can see a clear peak of fluorescence. Since the atomic beam goes in vertical and perpendicular to the PI laser direction and it is also limited by the holes in the oven shield, the Doppler shift is rather insignificant. There is also some dip in the PMT counts between 1 and 1.5 GHz detuning from f_0 . The reason is that the oven shield has barriers between the holes in the bottom. Therefore, there is a frequency that excites the transition of atoms with certain velocities, but which are blocked by the shield. To confirm this we shifted the PI laser a little around initial position. Results are shown in Fig. 8 (b).

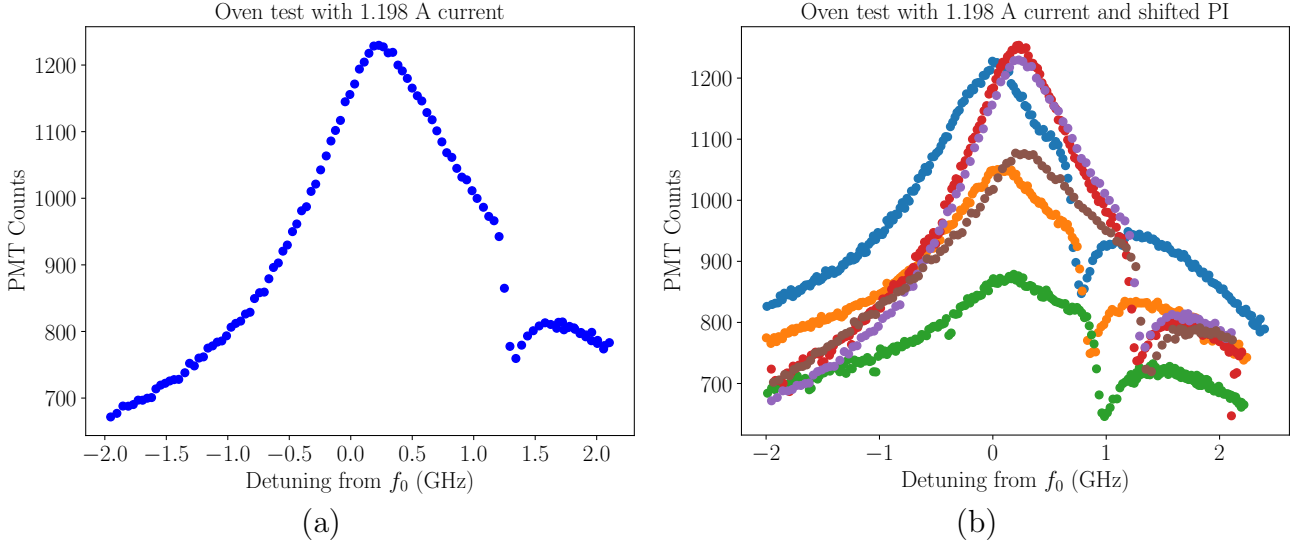


Figure 8: (a) – single fluorescence peak, (b) – fluorescence peaks for the different positions of PI laser

Due to the periodicity of the hole system, it is difficult to say exactly what is happening. But according to the displacement of the dip, we can understand that PI laser goes through the places where atoms with different velocities are blocked. The change in the height of the peaks indicates a different number of atoms in various places inside the chamber but also an absolute increase in number of atoms with higher current.

4.3 Ablation without collimator

Here we will describe the ablation experiments that were performed. In the first series of measurements we didn't use the collimator and used a thin wire (0.25 mm in diameter) as an ablation target. Let's now return to the sequence shown in Fig. 6. Since we want to analyze the behavior of atoms with different velocities, we will take measurements at different values of the arrival time. Similarly to the previous subsection, we will detune the frequency of the PI laser by changing the voltage on the piezo with an amplitude of 5 V. At every frequency step we will acquire data for different waiting times ranging from 140 to 250 μ s. Now we will run only one experiment with detection time of 2 μ s for every point of waiting time since it is time consuming to scan the whole range of frequencies. We will also only take a blue-shifted scan because the atomic beam and PI laser have a similar direction and if we use a red-shift, the back reflections from the chamber window might prevent us from observing a clear signal. Since we want to find the minimum required pulse energy of the ablation laser for generating atoms, we will make several measurements with different power settings of the 532 nm laser.

Thus, one series of measurements can take up to 30 minutes for every power value. Results are shown in Fig. 9.

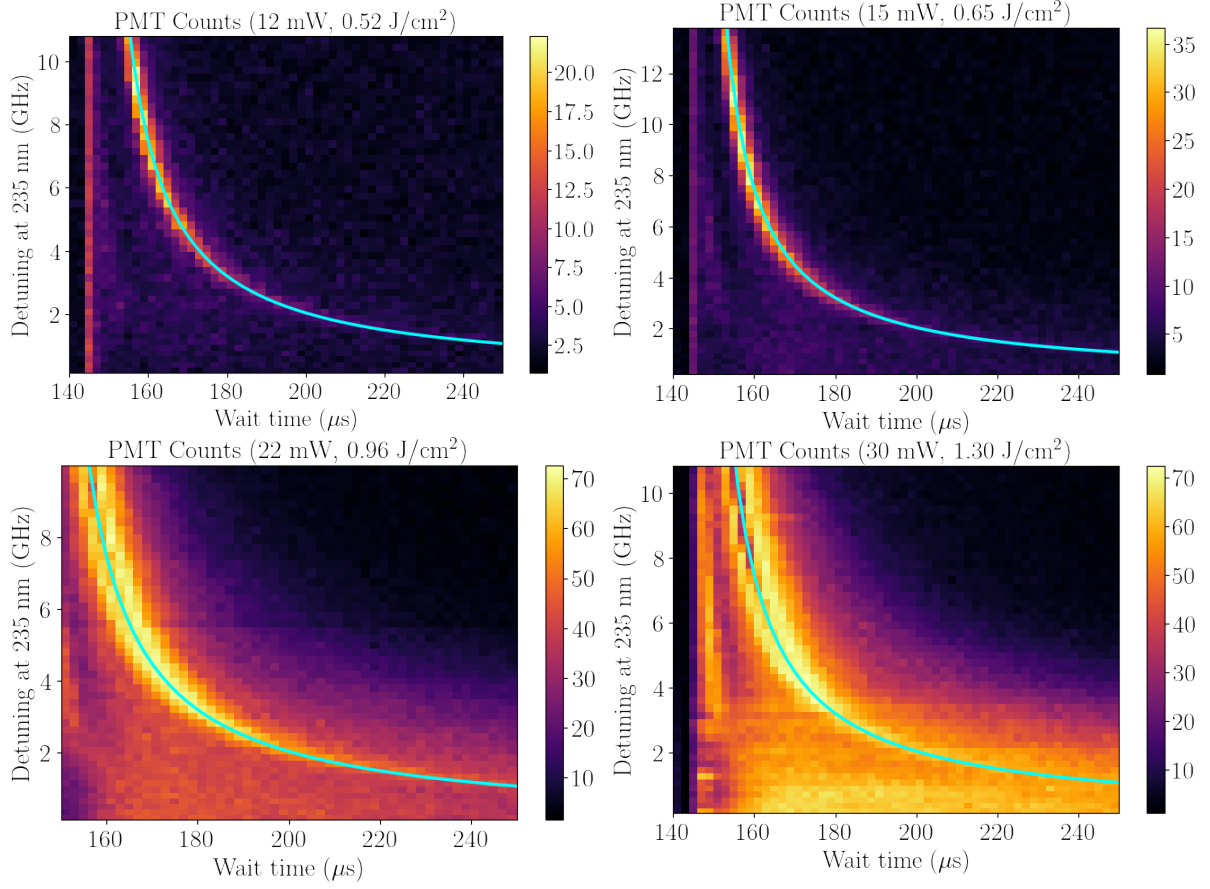


Figure 9: PMT counts dependent on PI detuning and waiting time with different ablation laser pulse energies. The color bar shows the number of counts which is different for each plot and the blue line is the overlaid theoretical curve given by Eq. (3).

The bright line at $145 \mu\text{s}$ is the flash of the ablation laser. As it will be mentioned in the section 5, we want to find the lowest achievable ablation laser power while we still can observe atoms. But on the two last plots (22 and 30 mW) you can see the rather huge part of very fast atoms between 150 and 170 μs . So at the power of 15 mW we also acquired the red-shifted scan which is shown in Fig. 10.

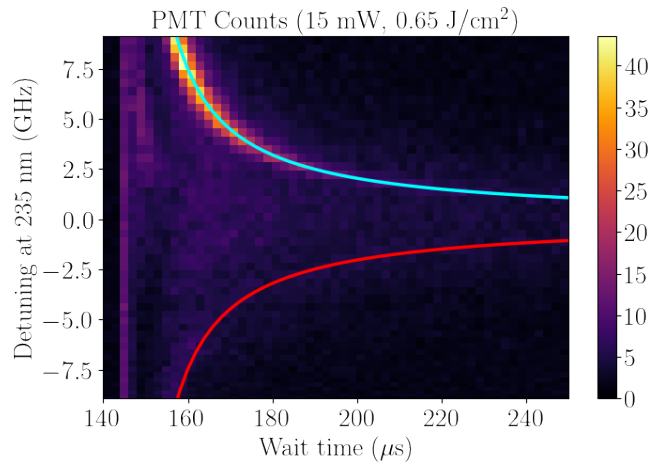


Figure 10: Full range scan with 15 mW of 532 light

Here we can see some part of slow atoms between 160 and 180 μs which probably could be captured and cooled. There also some slow atoms even in the middle of the wait time range near the resonant frequency. This phenomenon might be caused by collisions in the plasma. More detailed velocities values will be given in the subsection 5.1.

To analyse the contribution of the Doppler shift we also can plot the theoretical curve which is described by the following equation:

$$f_{obs} = f_{lab} \left(1 - \frac{v \cos \theta}{c} \right) = f_{lab} \left(1 - \frac{d \cos \theta}{ct_{arrival}} \right), \quad (3)$$

where f_{obs} is the laser frequency observed by the atom, f_{lab} the laser frequency in the lab frame, $v = d/t_{arrival}$ the velocity of the atoms, d the distance from the ablation target to the observation point (top of the needle), θ the angle between the PI beam and the atom velocities and c is the speed of the light in vacuum. Without the collimator we don't know the actual angle θ , but we estimate it from the CAD assembly to be around 21° .

4.4 Ablation with collimator

At the next step we put the collimator on the ablation target mount. Previously the wire was poorly mounted and under the influence of laser radiation, it was snapped. So we replaced this wire with a thicker one (1.2 mm in diameter) since such situation is highly undesirable in the real setup.

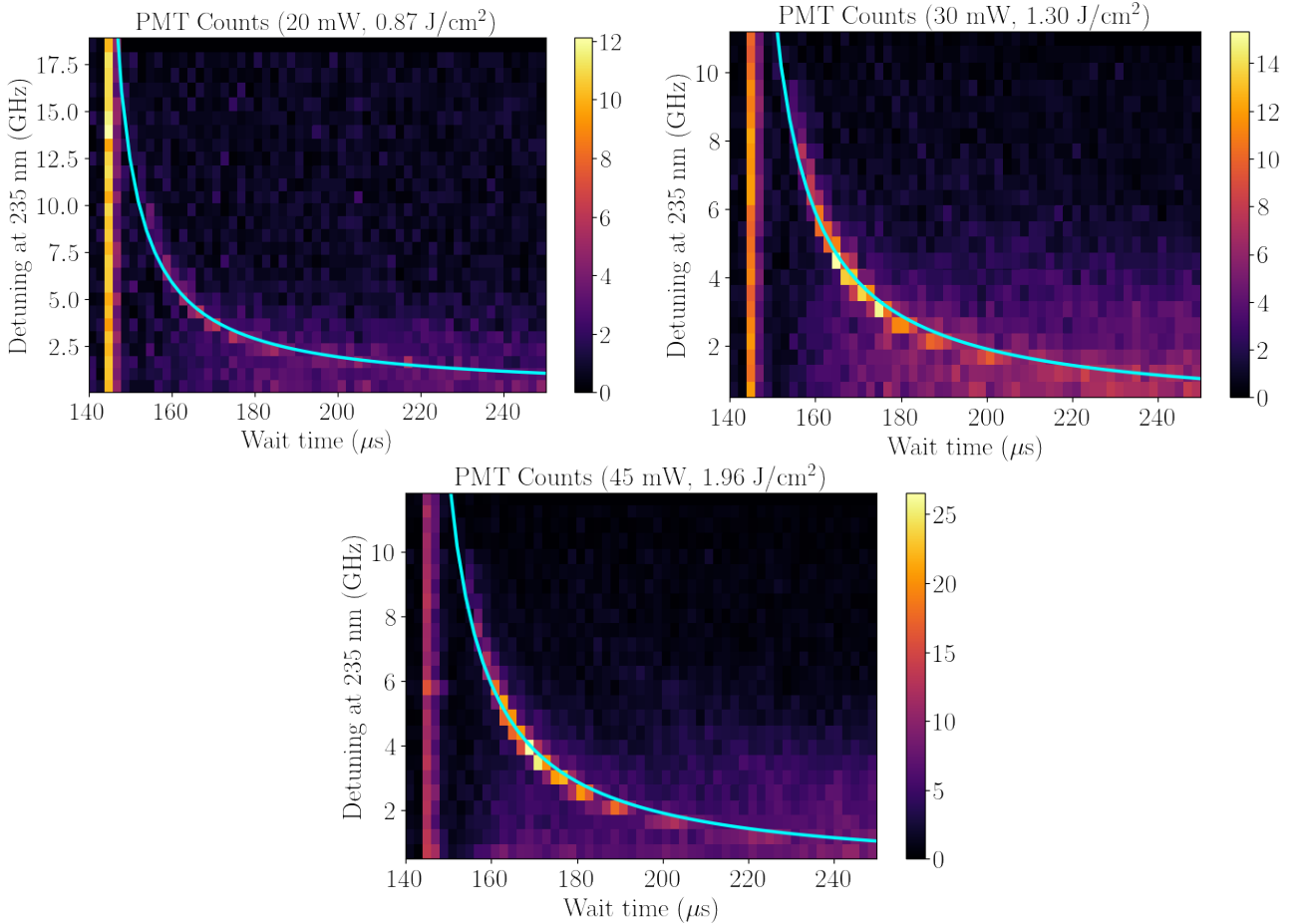


Figure 11: PMT counts dependence on PI detuning and waiting time with different power of ablation laser using collimator.

We also want to be sure that PI laser is aligned with a direction of the atoms we are able to observe, since the majority part of ablated particles are blocked by the collimator. So now the needle is fixed in the collimator and we have a selected direction of the beam with the angle of 24.8° between the atom flux and the PI beam and we can just align the PI laser with the top of the needle as in the case without the collimator. However, in this instance it is really difficult to align the laser beams so the efficiency of hitting the target is not optimal. Results are shown in Fig. 11.

In order to save time, the scan was performed with a larger range but with fewer samples. Now we have a very small number of fast atoms and a sufficient part of the slow atoms around the resonant frequency. We can also see a narrower Doppler shift line even at higher ablation laser powers, which makes sense since the gap in the collimator is 1 mm wide and only a really small part of the ablated atoms reaches the observation point.

5 Discussion

5.1 Speed distribution

The main reason for finding the lowest possible power of the ablation laser is that we expect to be more likely to trap and cool ions with velocities below 100 m s^{-1} in the real setup.

In order to obtain the frequency-independent velocity distribution of the ablation plume, we sum up the photon counts along each vertical line in Fig. 9 and Fig. 11 and convert the horizontal axis to velocity simply by $v = d/t$ where $d = 29 \text{ mm}$. Due to the fact that the transition $^1S_0 \longleftrightarrow ^1P_1$ is a closed transition, the PMT counts are considered inversely proportional to the atom velocity in the low intensity regime [6]. Therefore we need to rescale the PMT counts by multiplying their corresponding atom velocities to account for this effect. The final result is shown in Fig. 12.

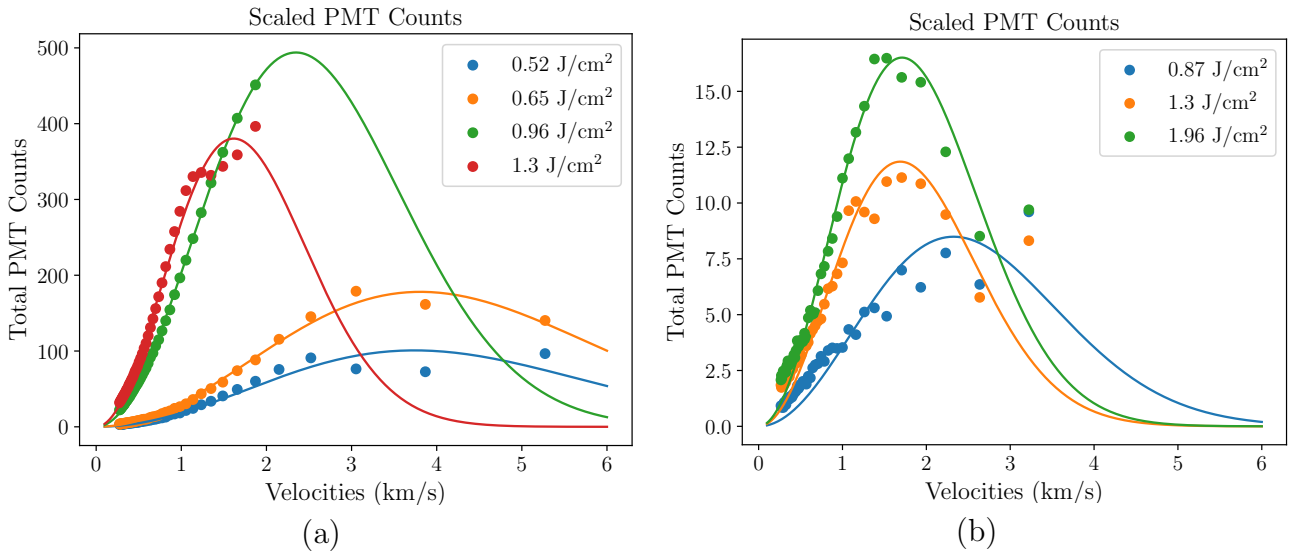


Figure 12: Velocities distribution: (a) – ablation without collimator, (b) – ablation with collimator

We fit this with the Maxwell-Boltzmann speed distribution:

$$N \cdot f_{\text{MB}}(v, T) = N \left(\frac{m}{2\pi kT} \right)^{3/2} 4\pi v^2 e^{-\frac{mv^2}{2kT}}, \quad (4)$$

where N is a scaling factor, T is a temperature in Kelvin, m is the beryllium atomic mass and k is the Boltzmann constant. From the approximation, we obtain the following values of atomic temperatures.

without collimator		with collimator	
Energy, J/cm ²	T , K	Energy, J/cm ²	T , K
1.96	–	1.96	1400
1.30	1400	1.30	1500
0.96	2900	0.87	2800
0.65	7600	0.65	–
0.52	7300	0.52	–

It may seem strange that the temperature increases when the laser power decreases. One of the limitations of our measurements was too low of a detuning to detect very fast atoms, so we missed most of them. Thus for example, the atomic velocity for a doppler shift of 10.2 GHz is 2.6 km/s so the data points above this value are not very indicative. Also, closer to higher power of ablation laser some part of beryllium ions might be produced by the fluence from which we cannot observe the proper fluorescence signal. However, this number, as a matter of fact, is not absolutely illustrative, due to the fact that the ablation scheme is not a thermalised process and hence there is no well defined temperature [6].

Reference [7] produced barium atoms with 1064 nm ablation laser and obtained a velocity distribution with several peaks. Unfortunately we don't have enough data at the large velocity end to state the same fact for our experiment for sure, but this might explain some of curves going back up at the end.

5.2 Ablation threshold

In addition to the fact that the collimator helps to obtain atoms with a limited range of velocities in the working area, it also has some disadvantages. Since we block some part of the atoms (and also due to the difference in illuminated surface when using the thicker wire) the threshold power increases. In our experiment we found the threshold near 0.52 J/cm² without the collimator using the 0.25 mm wire and around 0.87 J/cm² with the collimator and the 1.2 mm wire. In [8] it is mentioned that threshold for singly-charged ions lies just below 1.4 J/cm². The threshold from reference [9] was found near 0.7 J/cm² (peak fluence 1.4 J/cm²) and also a peak pulse fluence of 0.71 J/cm² was obtained in [10] for detecting beryllium atoms in a test using a residual gas analyser. And also just to be sure that our results are plausible we can compare them with [11] who gives the thresholds in range of 0.1–0.2 J/cm² for different metals (Ni, In, Cu, Mo, Au) as well as reference [12] found a threshold near 0.3 J/cm² for the production of calcium ions which have the same order of magnitude as our measurements.

In the [13] it is stated that with a thermally activated process no real threshold exists and we can generate ablated atoms significantly only above a certain fluence. That is also the reason why we could produce atoms at a lower threshold compared with a threshold for detecting ions which is described in [8].

Anyway it is hard to compare ablation experiments with each other, since the threshold depends quite strongly on the exact laser parameters such as frequency, pulse duration and the absolute size of the spot. [13].

6 Conclusion

In this paper, we have described the technique of producing ablated beryllium atoms. We also provided the results of detecting the ^9Be fluorescence that can be used for future loading of ions into a Penning trap. The possibility of excitation of atoms with suitable velocities for capture and cooling was experimentally shown as well as the ablation threshold was obtained. We also demonstrated successfully the correct operation of the setup, in a geometry similar to the one of the Penning trap setup.

References

- [1] R.J. Lewis-Swan et al. “Dynamics of quantum information”. In: *Nature Reviews Physics* 1 (2019), pp. 627–634. URL: <https://www.nature.com/articles/s42254-019-0090-y>.
- [2] J.W. Britton et al. “Engineered two-dimensional Ising interactions in a trapped-ion quantum simulator with hundreds of spins”. In: *Nature* 284 (2012), pp. 489–492. URL: <https://www.nature.com/articles/nature10981>.
- [3] E. Cook et al. “Testing Quantum Electrodynamics in the Lowest Singlet State of Neutral Beryllium-9”. In: *Physical Review Letters* 121 (2018). URL: <https://journals.aps.org/prl/abstract/10.1103/PhysRevLett.121.053001>.
- [4] S. Wolf et al. “Efficient and robust photo-ionization loading of beryllium ions”. In: *Applied Physics B* 124.30 (2018). URL: <https://link.springer.com/article/10.1007/s00340-018-6903-3>.
- [5] Guglielmo Coloretti. “Detecting the neutral fluorescence of ^9Be ”. In: *ETH Zürich, Trapped Ion Quantum Information group, Semester Project* (2021). URL: https://ethz.ch/content/dam/ethz/special-interest/phys/quantum-electronics/tiqi-dam/documents/semester_theses/semesterthesis-Guglielmo-Coloretti.
- [6] Peng Zhou. “Motional State Control and Ablation Loading in a Cryogenic Surface-Electrode Trap”. In: *ETH Zürich, Trapped Ion Quantum Information group, Master Thesis* (2017). URL: https://ethz.ch/content/dam/ethz/special-interest/phys/quantum-electronics/tiqi-dam/documents/masters_theses/masterthesis-Zhou-Peng.
- [7] M. Rossa, C. Rinaldi, and J. Ferrero. “Velocity distributions of Ba (1S_0 , 3D_J , 1D_2 , 3P_1 and 1P_1) and Ba^+ ($^2P_{3/2}$) produced by 1064 nm pulsed laser ablation of barium in vacuum”. In: *Journal of Applied Physics* 100 (2006). URL: <https://aip.scitation.org/doi/10.1063/1.2352807>.
- [8] M. Sameed, D. Maxwell, and N. Madsen. “Ion generation and loading of a Penning trap using pulsed laser ablation”. In: *New Journal of Physics* 22 (2020). URL: <https://iopscience.iop.org/article/10.1088/1367-2630/ab6066>.
- [9] Q. Wu et al. “Adaptively controlled fast production of defect-free beryllium ion crystals using pulsed laser ablation”. In: *Review of Scientific Instruments* 92 (2021). URL: <https://aip.scitation.org/doi/10.1063/5.0044372>.
- [10] Malte Niemann. “Design and commissioning of an experiment for sympathetic cooling and coupling of ions in a cryogenic Penning trap”. In: *Gottfried Wilhelm Leibniz Universität Hannover, Doctoral dissertation* (2019). URL: <https://www.repo.uni-hannover.de/handle/123456789/5376?locale-attribute=en>.

- [11] M.D. Shirk and P.A. Molian. “A review of ultrashort pulsed laser ablation of materials”. In: *Journal of Laser Applications* 10.18 (1998). URL: <https://lia.scitation.org/doi/10.2351/1.521827>.
- [12] K. Sheridan, W. Lange, and M. Keller. “All-optical ion generation for ion trap loading”. In: *Applied Physics B* 104.4 (2011). URL: <https://link.springer.com/article/10.1007/s00340-011-4563-7>.
- [13] Dieter Bäuerle. *Laser Processing and Chemistry*. URL: <https://link.springer.com/book/10.1007/978-3-642-17613-5>.